On the Application of Finite Methods in Time Domain to Anisotropic Dielectric Waveguides

Salvador González García, T. Materdey Hung-Bao, Rafael Gómez Martín, and Bernardo García Olmedo

Abstract—**This paper presents some general ideas for the construction of explicit finite algorithms to study wave propagation in dielectric anisotropic waveguides. The goal is to facilitate the development of different finite schemes through the extension of the finite-difference time-domain (FDTD) method to study anisotropic media. Some of these schemes are particularized and applied to the simulation of the propagation of electromagnetic waves through planar dielectric anisotropic waveguides.**

I. Introduction

THE FINITE-DIFFERENCE time-domain (FDTD) method has become one of the most effective tools for the numerical solution of Maxwell equations. It is based on the approximation of the derivatives by central differences and on the use of Yee's scheme to evaluate the field components [1]. The rapid growth of the literature on the subject is an indication of its general acceptance. It has been used to calculate the radar cross section (RCS) of complex objects to study the interaction of electromagnetic waves with living tissue, propagation through dispersive media, microwave circuits, antennas, propagation of solitons through nonlinear media, and dielectric optical waveguides. This wide range of applications is documented by the general references found in [2]–[30].

The application of finite methods to the treatment of optical-dielectric waveguides, which often include anisotropic media in their composition, is one area where this method can be successfully applied. Several variant versions of FDTD have recently been proposed [10]–[26] and the treatment of nondiagonal anisotropic media has been accomplished in different cases [4], [10], [11], [18], [22], [23].

This paper proposes a simple and systematic procedure to develop finite methods applicable to anisotropic media, particularly to optical integrated and microstrip waveguides.

Section II shows that the classical FDTD method cannot be straightforwardly applied to analyze anisotropic media. An operational language is introduced to simplify the application of finite methods to general anisotropic media. Section III describes algorithms for the time advancement of the values of the field components for Yee's grid and for several of its variants. The expressions are formulated operationally, so that their computer code can be automatically generated through the use of symbolic programs such as Mathematica. Section IV gives the basic ideas concerning dispersion and stability. Section V particularizes the results of Section III for two cases of planar anisotropic waveguides in birefringent media: one with the optical axis rotated in the plane of the slab and the other in a plane perpendicular to the plane of the slab. Finally, in Section VI the described methods are tested.

Manuscript received November 11, 1995; revised August 26, 1996. This work was supported in part by the National Research Project TIC-93-0671-C06-05.

The authors are with the Electromagnetic Group of Granada, Depto. Física Aplicada, Facultad de Ciencias, University of Granada, 18071 Granada, Spain.

Publisher Item Identifier S 0018-9480(96)08486-4.

II. Background

Starting from the traditional Yee algorithm, we first propose some variants that are suitable for the treatment of anisotropic media, and then we study the effects of fourth-order approximations of the derivatives.

Although the algorithms proposed herein are valid for any sort of time invariant linear anisotropic electric and/or magnetic material, for the sake of simplicity we will limit ourselves to inhomogeneous anisotropic dielectrics with dielectric tensor $\tilde{\varepsilon}$.

A. Maxwell Equations for Anisotropic Media

A convenient way to express the Maxwell curl equations in nonconductor anisotropic media is

$$\nabla \times \vec{E} = -\mu \frac{\partial \vec{H}}{\partial t} \tag{1}$$

$$\tilde{\xi} \cdot \nabla \times \vec{H} = \frac{\partial \vec{E}}{\partial t} \tag{2}$$

where $\tilde{\xi}$ is the inverse permittivity tensor $\tilde{\varepsilon}^{-1}$. The x component of (2) is

$$\frac{\partial E_x}{\partial t} = \xi_{xx}\left(\frac{\partial H_z}{\partial y} - \frac{\partial H_y}{\partial z}\right) + \left(\xi_{xy}\frac{\partial H_x}{\partial z} - \xi_{xz}\frac{\partial H_x}{\partial y}\right) + \left(\xi_{xz}\frac{\partial H_y}{\partial x} - \xi_{xy}\frac{\partial H_z}{\partial x}\right). \tag{3}$$

Observe that on the right-hand side of (3), three kinds of derivatives, which we call first, second, and third class derivatives, appear:

1) first class ($\partial H_z/\partial y$ and $\partial H_y/\partial z$): those multiplied by the diagonal element of $\tilde{\xi}$, which are the same as the ones in the isotropic case or when $\tilde{\xi}$ is diagonal;
2) second class ($\partial H_x/\partial y$ and $\partial H_x/\partial z$): those with the magnetic component along the direction of the electric field component (x) derived with respect to the perpendicular directions (y, z);

3) third class ($\partial H_y/\partial x$ and $\partial H_z/\partial x$): those with the magnetic components perpendicular to the direction of the electric field (y,z) derived with respect to the direction of the electric field (x).

Using second-order centered differences for the derivatives, at the points $\vec{P}_{E_x} \equiv (i+\frac{1}{2},j,k)\Delta$ and the times $t_H = (n+\frac{1}{2})\Delta t$ indicated by Yee's scheme [1]

$$\frac{\partial f(u,v,\cdots)}{\partial u} \simeq \frac{f\left(u+\frac{\Delta u}{2},v,\cdots\right)-f\left(u-\frac{\Delta u}{2},v,\cdots\right)}{\Delta u}$$

and denoting $\{E,H\}(i\Delta,j\Delta,k\Delta,n\Delta t) \equiv \{E,H\}^n(i,j,k)$, (3) can be approximated by[1]

$$\begin{aligned}
&\underbrace{E_x^{n+1}(i+\tfrac{1}{2},j,k)}\\
&\quad=\underbrace{E_x^n(i+\tfrac{1}{2},j,k)}+\frac{\Delta t}{\Delta}\{\xi_{xx}(\underbrace{H_z^{n+1/2}(i+\tfrac{1}{2},j+\tfrac{1}{2},k)}\\
&\qquad-\underbrace{H_z^{n+1/2}(i+\tfrac{1}{2},j-\tfrac{1}{2},k)}\\
&\qquad-\xi_{xx}(\underbrace{H_y^{n+1/2}(i+\tfrac{1}{2},j,k+\tfrac{1}{2})}\\
&\qquad-\underbrace{H_y^{n+1/2}(i+\tfrac{1}{2},j,k-\tfrac{1}{2})}\\
&\qquad+\xi_{xy}(H_x^{n+1/2}(i+\tfrac{1}{2},j,k+\tfrac{1}{2})\\
&\qquad-H_x^{n+1/2}(i+\tfrac{1}{2},j,k-\tfrac{1}{2}))\\
&\qquad-\xi_{xz}(H_x^{n+1/2}(i+\tfrac{1}{2},j+\tfrac{1}{2},k)\\
&\qquad-H_x^{n+1/2}(i+\tfrac{1}{2},j-\tfrac{1}{2},k))\\
&\qquad+\xi_{xz}(H_y^{n+1/2}(i+1,j,k)-H_y^{n+1/2}(i,j,k))\\
&\qquad-\xi_{xy}(H_z^{n+1/2}(i+1,j,k)-H_z^{n+1/2}(i,j,k))\}. \quad (4)
\end{aligned}$$

Notice that in (4), the only components actually present in Yee's grid [underbraced in (4) and shown in solid lines in Fig. 1] arise from the discretization of the first class derivatives. In order to treat the remaining components of (4) (in dashed lines in Fig. 1), it is clearly necessary to extend Yee's original scheme. In this paper we discuss three possible extensions.

1) The construction of an algorithm that only requires the components of Yee's cube, through a suitable approximation of the derivatives.
2) The modification of Yee's cube with the addition of the necessary components in order to use only centered differences.
3) The distribution of the components in a different way and the use of differences as well as means.

To make the process of building the finite schemes more systematic, some numerical operators will now be defined. This operational language is especially useful to implement the algorithms with symbolic calculus programs.

[1]Here and in the following we consider the usual explicit time advancing scheme of Yee's algorithm, which evaluates the electric field components at $t_E = n\Delta t$ and the magnetic ones at $t_H = (n+\frac{1}{2})\Delta t$, with n being an integer.

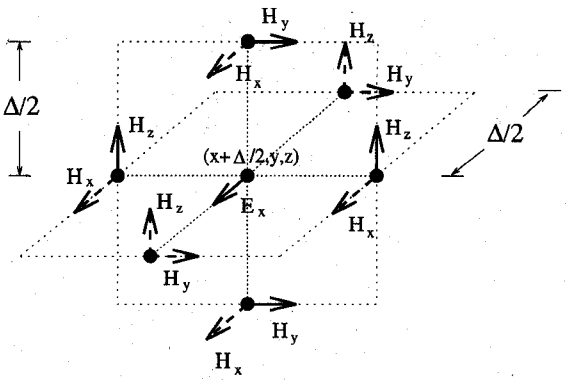

Fig. 1. Octant of Yee's grid completed with the components needed to compute E_x with only centered differences.

B. Finite Centered Operators

Consider a regular grid with nodes spaced in steps of $\Delta u/2$ and $f(u)$ sampled at each of its points. Let us define the *Shift Forward* F_u and *Shift Backward* B_u operators as

$$F_u \cdot f(u) = f\left(u+\frac{\Delta u}{2}\right)$$
$$B_u \cdot f(u) = f\left(u-\frac{\Delta u}{2}\right).$$

It is easy to show that they form a complete set of operators such that any other operator involving displacements in the variable can be obtained as a combination of them; therefore we term them *Fundamental Operators*. In particular, the *Centered Differentiation* operator is defined as

$$\begin{aligned}
D_u \cdot f(u) &= \frac{1}{\Delta u}(F_u \cdot f(u) - B_u \cdot f(u))\\
&= \frac{1}{\Delta u}\left(f\left(u+\frac{\Delta u}{2}\right)-f\left(u-\frac{\Delta u}{2}\right)\right) \quad (5)
\end{aligned}$$

which is a second-order approximation of the analytical partial differentiation operator. The *Centered Mean* operator is similarly defined as

$$\begin{aligned}
M_u \cdot f(u) &= \frac{1}{2}(F_u \cdot f(u) + B_u \cdot f(u))\\
&= \frac{1}{2}\left(f\left(u+\frac{\Delta u}{2}\right)+f\left(u-\frac{\Delta u}{2}\right)\right) \quad (6)
\end{aligned}$$

which can easily be shown to be a second-order approximation in Δu of the analytical identity operator. Both (5) and (6) are called *Basic Centered Operators*, since any other operator can also be obtained as a combination of them.

It is also helpful to define the operators D_{nu} and M_{nu} $(\forall n \geq 2)$, which evaluate the mean and the differentiation with points displaced $\pm(n\Delta u/2)$ in the direction u

$$\begin{aligned}
D_{nu} \cdot f(u) &= \frac{1}{n\Delta u}\left(f\left(u+\frac{n\Delta u}{2}\right)-f\left(u-\frac{n\Delta u}{2}\right)\right)\\
&= \frac{1}{n\Delta u}(F_u \circ \overset{n}{\cdots} \circ F_u - B_u \circ \overset{n}{\cdots} \circ B_u)\cdot f(u)\\
M_{nu} \cdot f(u) &= \frac{1}{2}\left(f\left(u+\frac{n\Delta u}{2}\right)+f\left(u-\frac{n\Delta u}{2}\right)\right)\\
&= \frac{1}{2}(F_u \circ \overset{n}{\cdots} \circ F_u + B_u \circ \overset{n}{\cdots} \circ B_u)\cdot f(u)
\end{aligned}$$

where $\circ$ denotes the composition of operators. To characterize the degree of approximation of the above operators let us apply them to functions of the form $f(u) = A\cos(ku)$ where $k = 2\pi/\lambda$ and λ represents the space or time period of $f(u)$. The relative error (ε_D) of the centered differentiation operator and that of the centered mean operator (ε_M), when they approximate the identity and the analytical partial derivative, respectively, may be bounded in the Taylor series expansion as

$$\varepsilon_M \equiv \left|\frac{f(u) - M_u \cdot f(u)}{f(u)}\right| = \frac{k^2(\Delta u)^2}{8} = \frac{4\pi^2}{8}\frac{1}{R_u^2}$$

$$\varepsilon_D \equiv \left|\frac{\dfrac{\partial f(u)}{\partial u} - D_u \cdot f(u)}{\dfrac{\partial f(u)}{\partial u}}\right| = \frac{\varepsilon_M}{3}$$

where $R_u = \lambda/\Delta u$ is the resolution of the variable u. It can be seen that the approximation is, in both cases, of second order in Δu.

The composition and linear combination of operators give rise to other operators with higher-order approximations. For instance, the Taylor series expansion of $f(u)$ up to fifth order in $\Delta u/2$ allows us to define the operators $\overline{M}_u$ and $\overline{D}_u$, shown in (7) and (8) at the bottom of the page, and which results in a fourth-order approximation of the analytical partial derivative and identity operators. When these operators are applied to the cosine-like functions, their error bounds are $\varepsilon_{\overline{M}} = \frac{3}{2}\varepsilon_M^2$ and $\varepsilon_{\overline{D}} = 0.2\varepsilon_{\overline{M}}$

III. Application of Finite Methods to Study Wave Propagation in Anisotropic Media

The FDTD method, like the extensions considered above, does not place all the field components at each node of a regular grid, but instead uses a staggered distribution of the components that allows the saving of memory and computation time. Consequently, for a given distribution of components, only the operators that use those components are compatible with that distribution. The set formed by the distribution of the field components and the compatible operators employed is called the *numerical scheme* of a finite method. Using the operational language described in the previous section, the extensions proposed in Section II-A are detailed in this section.

A. Schemes that Use Yee's Distribution of the Components

The purpose of this extension is to use only the components placed at the positions of Yee's grid (Fig. 2) to approximate Maxwell's curl equations. As can be seen in (4), the first class derivatives can be replaced by the centered differentiation operator. For the second and third class derivatives it is necessary to combine the centered mean operator with the centered differentiation operator to obtain a scheme only involving the components defined in Yee's grid. This can be carried out in the following way:

1) Second class derivatives (for instance $\partial H_x/\partial z$ in $\vec{P}_{E_x}$): as the operator D_z needs, for instance, the value $H_x(\vec{P}_1)$ (see Fig. 2), it can be obtained by applying the operators M_y and M_x to average the nearest four components. So the following operators are needed

$$D_x^* \equiv D_x \circ M_y \circ M_z, \qquad D_y^* \equiv D_y \circ M_x \circ M_z$$
$$D_z^* \equiv D_z \circ M_x \circ M_y. \tag{9}$$

2) Third class derivatives (for instance $\partial H_y/\partial x$ in $\vec{P}_{E_x}$): as D_x needs, for instance, $H_y(\vec{P}_2)$, it is necessary to differentiate in x and average in x and in z, so let us define

$$D_{x(z)}^* \equiv D_x \circ M_x \circ M_z = D_{2x} \circ M_z$$
$$D_{x(y)}^* \equiv D_x \circ M_x \circ M_y = D_{2x} \circ M_y \tag{10}$$
$$D_{y(x)}^* \equiv D_y \circ M_y \circ M_x = D_{2y} \circ M_x$$
$$D_{y(z)}^* \equiv D_y \circ M_y \circ M_z = D_{2y} \circ M_z \tag{11}$$
$$D_{z(x)}^* \equiv D_z \circ M_z \circ M_x = D_{2z} \circ M_x$$
$$D_{z(y)}^* \equiv D_z \circ M_z \circ M_y = D_{2z} \circ M_y. \tag{12}$$

At the points of Yee's grid

$$\vec{P}_{E_x} \equiv (i+\tfrac{1}{2}, j, k), \qquad \vec{P}_{E_y} \equiv (i, j+\tfrac{1}{2}, k),$$
$$\vec{P}_{E_z} \equiv (i, j, k+\tfrac{1}{2}) \qquad \vec{P}_{H_x} \equiv (i, j+\tfrac{1}{2}, k+\tfrac{1}{2}),$$
$$\vec{P}_{H_y} \equiv (i+\tfrac{1}{2}, j, k+\tfrac{1}{2}), \qquad \vec{P}_{H_z} \equiv (i+\tfrac{1}{2}, j+\tfrac{1}{2}, k)$$

the discretized Maxwell's curl equations become (13), shown at the bottom of the next page, and

$$\begin{aligned} D_t \cdot E_y^{n+1/2}(\vec{P}_{E_y}) &= \xi_{yy}(D_z \cdot H_x^{n+1/2}(\vec{P}_{E_y}) - D_x \cdot H_z^{n+1/2}(\vec{P}_{E_y})) \\ &\quad + (\xi_{yz} D_x^* \cdot H_y^{n+1/2}(\vec{P}_{E_y}) \\ &\quad - \xi_{yx} D_z^* \cdot H_y^{n+1/2}(\vec{P}_{E_y})) \\ &\quad + (\xi_{yx} D_{y(x)}^* \cdot H_z^{n+1/2}(\vec{P}_{E_y}) \\ &\quad - \xi_{yz} D_{y(z)}^* \cdot H_x^{n+1/2}(\vec{P}_{E_y})) \end{aligned} \tag{14}$$

$$\overline{D}_u \cdot f(u) \equiv \frac{9D_u - D_{3u}}{8} \cdot f(u) = \frac{\left[27\left(f\left(u+\frac{\Delta u}{2}\right) - f\left(u-\frac{\Delta u}{2}\right)\right) - \left(f\left(u+\frac{3\Delta u}{2}\right) - f\left(u-\frac{3\Delta u}{2}\right)\right)\right]}{24\Delta u} \tag{7}$$

$$\overline{M}_u \cdot f(u) \equiv \frac{9M_u - M_{3u}}{8} \cdot f(u) = \frac{\left[9\left(f\left(u+\frac{\Delta u}{2}\right) + f\left(u-\frac{\Delta u}{2}\right)\right) - \left(f\left(u+\frac{3\Delta u}{2}\right) + f\left(u-\frac{3\Delta u}{2}\right)\right)\right]}{16} \tag{8}$$

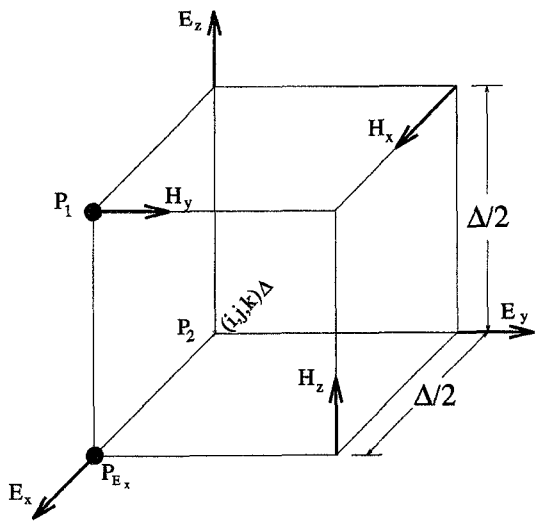

Fig. 2. Octant of the three-dimensional (3-D) Yee's grid.

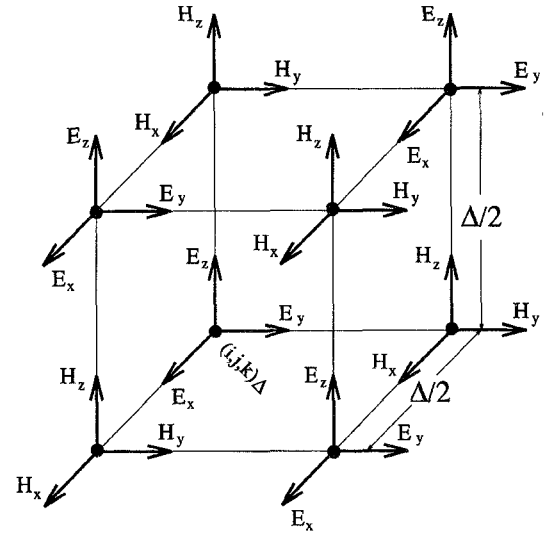

Fig. 3. Octant of the 3-D condensed two-node grid.

$$
\begin{aligned}
&D_t \cdot E_z^{n+1/2}(\vec{P}_{E_z}) \\
&\quad = \xi_{zz}(D_x \cdot H_y^{n+1/2}(\vec{P}_{E_z}) - D_y \cdot H_x^{n+1/2}(\vec{P}_{E_z})) \\
&\qquad + (\xi_{zx} D_y^* \cdot H_z^{n+1/2}(\vec{P}_{E_z}) \\
&\qquad - \xi_{zy} D_x^* \cdot H_z^{n+1/2}(\vec{P}_{E_z})) \\
&\qquad + (\xi_{zy} D_{z(y)}^* \cdot H_x^{n+1/2}(\vec{P}_{E_z}) \\
&\qquad - \xi_{zx} D_{z(x)}^* \cdot H_y^{n+1/2}(\vec{P}_{E_z}))
\end{aligned} \tag{15}
$$

$$\mu D_t \cdot H_x^n(\vec{P}_{H_x}) = (D_z \cdot E_y^n(\vec{P}_{H_x}) - D_y \cdot E_z^n(\vec{P}_{H_x})) \tag{16}$$

$$\mu D_t \cdot H_y^n(\vec{P}_{H_y}) = (D_x \cdot E_z^n(\vec{P}_{H_y}) - D_z \cdot E_x^n(\vec{P}_{H_y})) \tag{17}$$

$$\mu D_t \cdot H_z^n(\vec{P}_{H_z}) = (D_y \cdot E_x^n(\vec{P}_{H_z}) - D_x \cdot E_y^n(\vec{P}_{H_z})). \tag{18}$$

Observe that although this scheme only uses the components defined in Yee's cube, it treats each derivative in a different manner.

The fourth-order operators defined in (7) and (8) can alternatively be used in the above expressions in order to obtain a fourth-order approximation of the derivatives. As will then be shown, the resulting algorithm has less phase dispersion than that of the second-order approximation without additional memory requirements, and it only requires some more computation time. This is especially convenient to treat large problems.

It can easily be shown that the bound error of the operators D_u^* and $D_{u(v)}^*$ is $7\varepsilon_D$ and that of $\overline{D}_u^*$ and $\overline{D}_{u(v)}^*$ is $11\varepsilon_{\overline{D}}$, where ε_D is the bound error of D_u, and $\varepsilon_{\overline{D}}$ that of $\overline{D}_u$.

B. Schemes that Only Use Centered Differences

The second extension proposed places the components in such a way that only the Centered Differentiation operator D_u $(u = \{x, y, z\})$ defined in (5) is used to replace all the derivatives. The octant of the spatial grid that allows this is illustrated in Fig. 3. This grid, henceforth called *condensed two-node* grid, has a density of 24 components per cell as opposed to the six components per cell of Yee's grid. That is, each component is placed at four different locations within each octant, so, although in principle this extension seems advantageous, the memory and computation time requirements are four times those of Yee. Nevertheless, it will be shown below that a particularization to a two-dimensional (2-D) case does not need either additional memory or computation time.

C. Other Schemes

The last extension is based on the placing of all the electric field components at one node of the grid and all the magnetic field components at the opposite node [14]. Fig. 4 shows the octant of this grid, which will henceforth be called *two-node* grid. It requires the same number of components per cell as that of Yee (six), and the advancing algorithm is obtained upon substitution of all the spatial derivatives by the operators D_u^*

$$
\begin{aligned}
D_t \cdot E_x^{n+1/2}(\vec{P}_{E_x}) = \overbrace{\xi_{xx}(D_y \cdot H_z^{n+1/2}(\vec{P}_{E_x}) - D_z \cdot H_y^{n+1/2}(\vec{P}_{E_x}))}^{\text{(first class)}} + \underbrace{(\xi_{xy} D_z^* \cdot H_x^{n+1/2}(\vec{P}_{E_x}) - \xi_{xz} D_y^* \cdot H_x^{n+1/2}(\vec{P}_{E_x}))}_{\text{(second class)}} \\
+ \underbrace{(\xi_{xz} D_{x(z)}^* \cdot H_y^{n+1/2}(\vec{P}_{E_x}) - \xi_{xy} D_{x(y)}^* \cdot H_z^{n+1/2}(\vec{P}_{E_x}))}_{\text{(third class)}}
\end{aligned} \tag{13}
$$

TABLE I
CRITICAL VALUES OF THE COURANT NUMBER C

	Two dimensions	Three dimensions
Second order two–node	1	1
Fourth order two–node	$\frac{6}{7}$	$\frac{6}{7}$
Second order condensed two–node	$\frac{1}{\sqrt{2}}$	$\frac{1}{\sqrt{3}}$
Fourth order condensed two–node	$\frac{6}{7\sqrt{2}}$	$\frac{6}{7\sqrt{3}}$

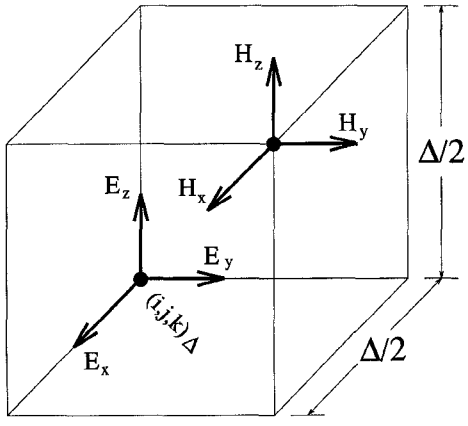

Fig. 4. Octant of the 3-D two-node grid.

defined in (9) at the points

$$\vec{P}_{E_u} \equiv (i,j,k), \quad \vec{P}_{H_u} \equiv (i+\tfrac{1}{2}, j+\tfrac{1}{2}, k+\tfrac{1}{2})$$

with $u = \{x, y, z\}$. In the same way the operators defined in (7) and (8) can be used to obtain a fourth-order algorithm.

IV. NUMERICAL DISPERSION AND STABILITY

This section looks at the numerical stability conditions and dispersion characteristics. The starting point for both is the establishment of the dispersion relation from the wave equations. For this purpose let us write Ampere's law in matrix form, for anisotropic media

$$\tilde{\xi} \cdot \tilde{R} \cdot \vec{H} = \frac{\partial \vec{E}}{\partial t}$$

and Faraday's law

$$-\tilde{R} \cdot \vec{E} = \mu \frac{\partial \vec{H}}{\partial t}$$

with the curl operator $\tilde{R}$ given by

$$\tilde{R} = \begin{pmatrix} 0 & -\frac{\partial}{\partial z} & \frac{\partial}{\partial y} \\ \frac{\partial}{\partial z} & 0 & -\frac{\partial}{\partial x} \\ -\frac{\partial}{\partial y} & \frac{\partial}{\partial x} & 0 \end{pmatrix}$$

and the wave equations by

$$\left(\tilde{R} \cdot \tilde{\xi} \cdot \tilde{R} + \mu \frac{\partial^2}{\partial t^2}\right)\vec{H} = 0, \quad \left(\tilde{\xi} \cdot \tilde{R} \cdot \tilde{R} + \mu \frac{\partial^2}{\partial t^2}\right)\vec{E} = 0.$$

Both wave equations lead to the same dispersion relation, which is here expressed as an eigenvalue problem

$$|\tilde{\Lambda} \cdot \tilde{\xi} \cdot \tilde{\Lambda} + \mu \lambda_t^2 \tilde{I}| = 0$$

where $\tilde{\Lambda}$ is the eigenvalue matrix of the curl operator, λ_t is the eigenvalue of the time derivative operator, and $\tilde{I}$ is the identity operator. A similar procedure can be followed in the numerical case, with $\tilde{\Lambda}$ now being the eigenvalue matrix of the numerical curl operator and λ_t the eigenvalue of D_t. If the numerical curl applied to $\vec{E}$ is different from that applied to $\vec{H}$, the dispersion relation is obtained from

$$|\tilde{\Lambda}^E \cdot \tilde{\xi} \cdot \tilde{\Lambda}^H + \mu \lambda_t^2 \tilde{I}| = 0$$

with $\tilde{\Lambda}^E$ and $\tilde{\Lambda}^H$ being the eigenvalue matrices of the different numerical curls.

Since the defined operators have the following eigenvalues, for eigenvectors of the form $f(u) = e^{jk_u u}$

$$D_u \mapsto \frac{2j}{\Delta u} \sin\left(k_u \frac{\Delta u}{2}\right), \quad M_u \mapsto \cos\left(k_u \frac{\Delta u}{2}\right)$$

and taking into account the algebraic properties of the eigenvalues of composed operators, all the numerical dispersion relations can be derived. Once λ_t has been obtained, the Von-Neumann condition gives the stability criterion

$$\mathrm{Re}(\lambda_t) = 0, \quad |\mathrm{Im}(\lambda_t)| \leq \frac{2}{\Delta t}.$$

Defining the Courant number in free space as $C = c\Delta t/\Delta$, the critical number under which the different schemes become unstable is shown in Table I. It can be seen that the stability condition of Yee's scheme is the same as that of the condensed two-node scheme since both schemes coincide in the isotropic case. These stability conditions always provide upper bounds for the stability conditions of the general anisotropic case.

V. APPLICATION TO THE PROPAGATION OF MODES ON SYMMETRIC SLAB OPTICAL WAVEGUIDES

To study and demonstrate the performance of the previously described methods we have chosen the two examples described in [27] and [28] by Marcuse, which study the 2-D propagation of waves on planar anisotropic uniaxial waveguides. In the first case [27] the optical axis is not contained in the plane of the slab, and in the second [28] the slab is coplanar with the optical axis. Fig. 5 shows the structure of these waveguides. They are formed by three slabs of anisotropic materials. The central one (guide) has width $2d$ and a dielectric tensor $\tilde{\varepsilon}^g$

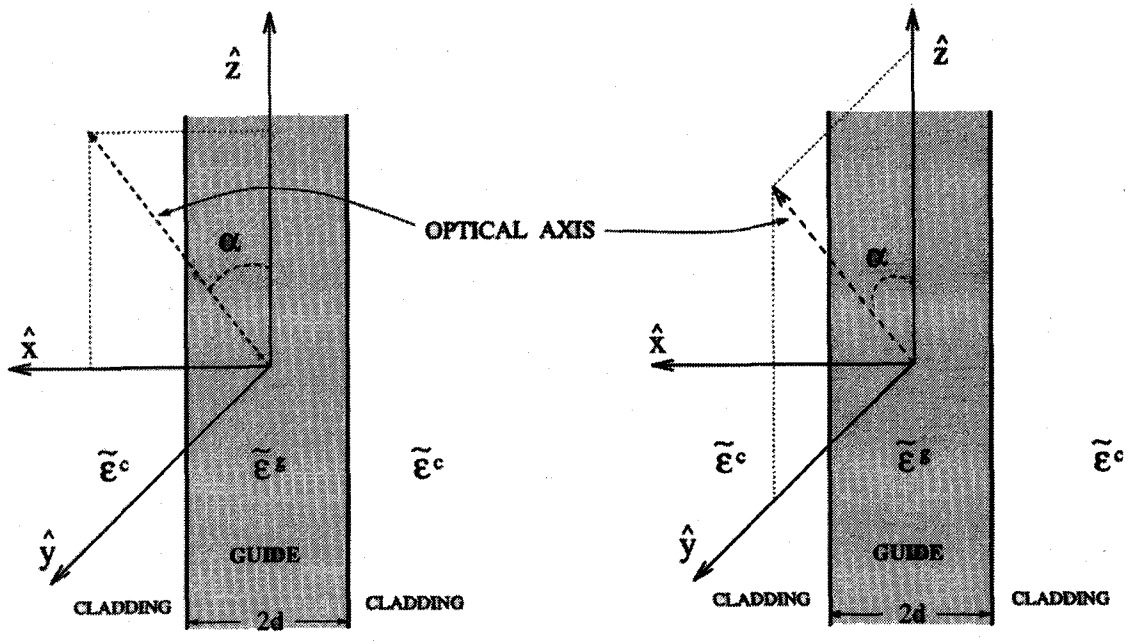

Fig. 5. Structure of the anisotropic waveguides.

with the optical axis forming an angle α with the z axis. It is placed between two slabs (cladding) with a dielectric tensor $\tilde{\varepsilon}^c$ with an optical axis parallel to that of the guide. In the first case the optical axis is rotated in the XZ plane, and in the second in the YZ plane. This type of guide can be obtained, for instance, by the diffusion of metals into lithium niobate.

The waveguide is illuminated with a He-Ne laser with a free space wavelength $\lambda_0 = 0.6328$ μm ($\omega = 2.977 \cdot 10^{15}$ rad/seg., $k = 9.929$ μm^{-1}) along the z axis with modes that are independent of the y coordinate.

Given the invariance of fields along the the y axis ($\partial/\partial y = 0$), the operators needed to simulate this problem are the centered differentiation (5) and the following simplifications of (9)–(12):

$$D_x^* \equiv D_x \circ M_z, \quad D_z^* \equiv D_z \circ M_x \tag{19}$$

$$D_{x(z)}^* \equiv D_x \circ M_x \circ M_z = D_{2x} \circ M_z$$

$$D_{x(y)}^* \equiv D_x \circ M_x = D_{2x} \tag{20}$$

$$D_{z(x)}^* \equiv D_z \circ M_z \circ M_x = D_{2z} \circ M_x$$

$$D_{z(y)}^* \equiv D_z \circ M_z = D_{2z}. \tag{21}$$

A. Optical Axis Not in the Plane of the Slab

The inverse dielectric tensor of a uniaxial material, with respect to its principal axes, is

$$\tilde{\xi}' = \begin{pmatrix} \xi_1 & 0 & 0 \\ 0 & \xi_1 & 0 \\ 0 & 0 & \xi_3 \end{pmatrix}$$

where $\xi_1 = 1/\varepsilon_1, \xi_3 = 1/\varepsilon_3$ and the optical axis lies along z. If the optical axis is rotated α in the XZ plane and $\tilde{T}$ is the rotation matrix

$$\tilde{\xi} = \tilde{T}^t \tilde{\xi}' \tilde{T} = \begin{pmatrix} \xi_{xx} & 0 & \xi_{xz} \\ 0 & \xi_{yy} & 0 \\ \xi_{xz} & 0 & \xi_{zz} \end{pmatrix}.$$

This rotation breaks the symmetry of the problem with respect to the plane $x = 0$, so that there are no truly symmetric or antisymmetric modes. Nevertheless "symmetric" or "antisymmetric" H_y modes are defined[2] where the amplitude, not the phase, of that component has the required symmetry. More details can be found in [27].

As a consequence of $\tilde{\xi}$ being symmetric and $\xi_{xy} = \xi_{zy} = 0$, (1) and (2) are uncoupled in two sets: one for the TE polarization, which corresponds to an ordinary mode analogous to that of isotropic materials, and the other for TM, which corresponds to an extraordinary mode. This latter relates the components H_y, E_x and E_z by

$$\frac{\partial E_x}{\partial t} = \left(\xi_{xz} \frac{\partial}{\partial x} - \xi_{xx} \frac{\partial}{\partial z} \right) H_y$$

$$\frac{\partial E_z}{\partial t} = \left(\xi_{zz} \frac{\partial}{\partial x} - \xi_{xz} \frac{\partial}{\partial z} \right) H_y$$

$$\mu \frac{\partial H_y}{\partial t} = \frac{\partial E_z}{\partial x} - \frac{\partial E_x}{\partial z}.$$

These equations involve what we previously termed first and third class derivatives. The schemes described in Section III can easily be particularized from the 3-D case, taking into account the operators (5), (19)–(21), and the particularizations of the grids of Figs. 2–4, as described below.

1) Yee's grid is obtained by spatially distributing the components in a plane section Yee's cube, as in Fig. 6(a).
2) The components of the bidimensional version of the *condensed two-node* grid are placed according to Fig. 6(b). Its memory requirement is twice that of the other two alternatives.
3) Finally, the bidimensional *two-node* grid distributes the components as in Fig. 6(c).

[2]In "symmetric" H_y modes, H_y and E_x are "symmetric" and E_z is "antisymmetric."

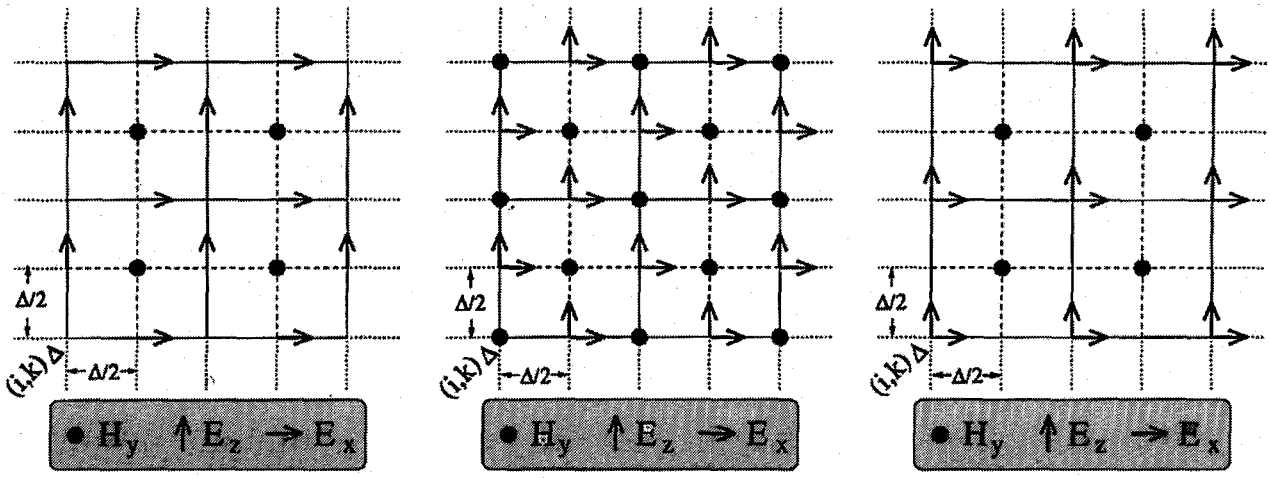

Fig. 6. Particularizations of the 3-D grids to treat bidimensional propagation in an anisotropic medium with its optical axis not coplanar with the medium. (a) Yee's grid. (b) Condensed two-node grid. (c) Two-node grid.

The first and third grids have a density of three components per cell, whereas the second one has six components per cell.

B. Optical Axis in the Plane of the Slab

In this case the optical axis is rotated in the YZ plane, and so the problem presents symmetry with respect to the plane $x = 0$ and the solutions can be expressed in terms of symmetric and antisymmetric H_y modes.[3]

The rotated dielectric tensor has the form

$$\tilde{\xi} = \begin{pmatrix} \xi_{xx} & 0 & 0 \\ 0 & \xi_{yy} & \xi_{yz} \\ 0 & \xi_{yz} & \xi_{zz} \end{pmatrix}.$$

Then, (1) and (2) are not uncoupled, and it is necessary to use the six field components together

$$\begin{aligned} \frac{\partial E_x}{\partial t} &= -\xi_{xx}\frac{\partial H_y}{\partial z} \\ \frac{\partial E_y}{\partial t} &= \xi_{yy}\left(\frac{\partial H_x}{\partial z} - \frac{\partial H_z}{\partial x}\right) + \xi_{yz}\frac{\partial H_y}{\partial x} \\ \frac{\partial E_z}{\partial t} &= \xi_{yz}\left(\frac{\partial H_x}{\partial z} - \frac{\partial H_z}{\partial x}\right) + \xi_{zz}\frac{\partial H_y}{\partial x} \\ \mu\frac{\partial H_x}{\partial t} &= \frac{\partial E_y}{\partial z} \\ \mu\frac{\partial H_y}{\partial t} &= \frac{\partial E_z}{\partial x} - \frac{\partial E_x}{\partial z} \\ \mu\frac{\partial H_z}{\partial t} &= -\frac{\partial E_y}{\partial x}. \end{aligned}$$

These expressions involve first, second, and third class derivatives. The three solutions proposed in Section III are concretized for this case by the operators (5), (19)–(21), and a particularization of Figs. 2–4 in the following way.

1) Although there is no bi-dimensional section of Yee's cube containing the six field components, it is possible to collapse two sections in the y direction to obtain the distribution of Fig. 7(a). The algorithm that makes use of only those components is the direct particularization of the 3-D one.
2) The *condensed two-node* grid places its components as illustrated in Fig. 7(b). As opposed to the general 3-D case, no additional memory or computation time is required because only six of the components are needed in each octant.
3) Finally the bi-dimensional *two-node* grid is obtained by collapsing two sections of the 3-D grid, as can be seen in Fig. 7(c).

All three grids have a density of six components per cell.

[3] In symmetric H_y modes, H_y, H_z, and E_x are symmetric and E_y, E_z, and H_x are antisymmetric

VI. Results

This section shows the results for the waveguides described in Section V. Given the diversity of possible schemes, the tests have been limited to those that use the same operator for all the components with comparable memory requirements. For the first case (optical axis not in the plane of the slab) results for second- and fourth-order two-node schemes are presented, for the sake of example. The second case (optical axis in the plane of the slab) has been simulated with second- and fourth order two-node and condensed two-node schemes. The theoretical values of the fields used for comparison are given in detail in [27] and [28].

A. Optical Axis Not in the Plane of the Slab

In this case a "symmetric" H_y mode has been used. The amplitudes of these modes are [27]

$$H_y = \begin{cases} A\cos(\kappa d)e^{-j\sigma d}e^{\gamma(x+d)}e^{j(\rho(x+d)-\beta z)}e^{j\omega t} \\ \quad \text{for } x \le -d \\ A\cos(\kappa x)e^{j(\sigma x-\beta z)}e^{j\omega t} \\ \quad \text{for } |x| \le d \\ A\cos(\kappa d)e^{j\sigma d}e^{-\gamma(x-d)}e^{j(\rho(x-d)-\beta z)}e^{j\omega t} \\ \quad \text{for } x \ge d \end{cases} \tag{22}$$

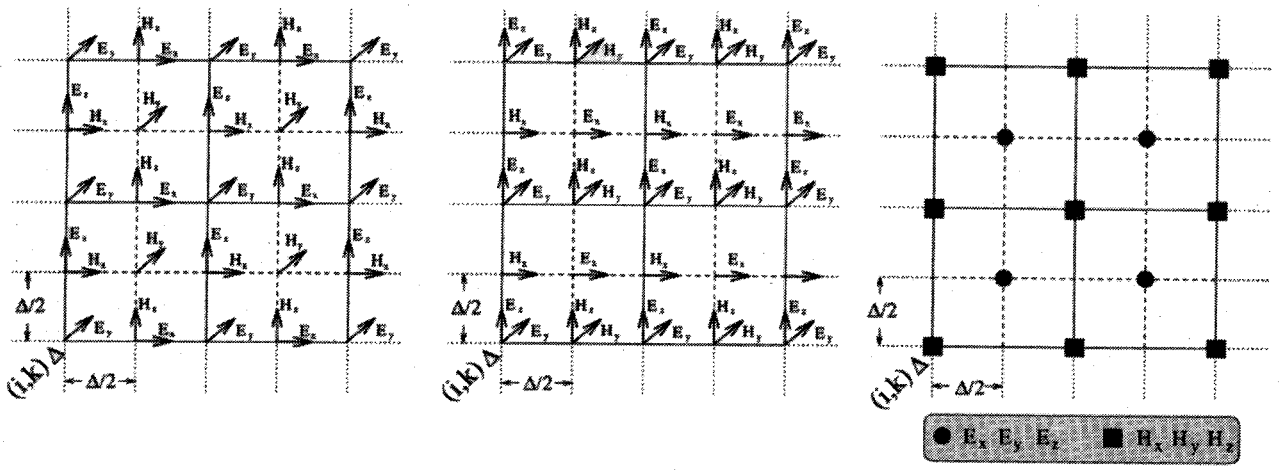

(a) (b) (c)

Fig. 7. Particularizations of the 3-D grids to treat bidimensional propagation in an anisotropic medium with its optical axis coplanar with the medium. (a) Yee's grid. (b) Condensed two-node grid. (c) Two-node grid.

$$E_x = \begin{cases} \dfrac{j}{\omega\eta^g}\left(\varepsilon^g_{xz}\dfrac{\partial H_y}{\partial x} - j\beta\varepsilon^g_{zz}H_y\right) & \text{for } |x| < d \\ \dfrac{j}{\omega\eta^c}\left(\varepsilon^c_{xz}\dfrac{\partial H_y}{\partial x} - j\beta\varepsilon^c_{zz}H_y\right) & \text{for } |x| > d \end{cases} \tag{23}$$

$$E_z = \begin{cases} \dfrac{-j}{\omega\eta^g}\left(\varepsilon^g_{xx}\dfrac{\partial H_y}{\partial x} - j\beta\varepsilon^g_{xz}H_y\right) & \text{for } |x| < d \\ \dfrac{-j}{\omega\eta^c}\left(\varepsilon^c_{xx}\dfrac{\partial H_y}{\partial x} - j\beta\varepsilon^c_{xz}H_y\right) & \text{for } |x| > d \end{cases} \tag{24}$$

where A is an arbitrary amplitude and

$$\eta^g = \varepsilon^g_{xx}\varepsilon^g_{zz} - (\varepsilon^g_{xz})^2, \quad \eta^c = \varepsilon^c_{xx}\varepsilon^c_{zz} - (\varepsilon^c_{xz})^2$$

$$\beta = \sqrt{\frac{\varepsilon^g_{xx}}{\varepsilon_0}k^2 - \frac{(\varepsilon^g_{xx})^2}{\eta^g}\kappa^2}, \quad \gamma = \sqrt{\frac{\eta^c}{(\varepsilon^c_{xx})^2}\left(\beta^2 - \frac{\varepsilon^c_{xx}}{\varepsilon_0}k^2\right)}$$

$$\sigma = \frac{\varepsilon^g_{xz}}{\varepsilon^g_{xx}}\beta, \quad \rho = \frac{\varepsilon^c_{xz}}{\varepsilon^c_{xx}}\beta$$

and κ is obtained from the eigenvalue equation

$$\eta^g\gamma\varepsilon^c_{xx}\cos(\kappa d) - \eta^c\kappa\varepsilon^g_{xx}\sin(\kappa d) = 0.$$

The parameters of the guide have been set at the values: width of the guide $2d = 1.274\ \mu\text{m}, \alpha = 30°$, ordinary refractive index in the cladding $n_{co} = \sqrt{\varepsilon^c_1/\varepsilon_0} = 2.383$, extraordinary one $n_{ce} = \sqrt{\varepsilon^c_3/\varepsilon_0} = 2.294$, and dielectric constants of the guide $\varepsilon^g_i = \varepsilon^c_i(1+\delta)$, with $i = \{1,3\}$ and $\delta = 0.1$, *viz.*, refractive indexes of the guide $n_{go} = \sqrt{1.1}n_{co}$ and $n_{ge} = \sqrt{1.1}n_{ce}$. The mode chosen corresponds to the root $\beta = 2.335 \cdot 10^7$ (wavelength $\lambda = 0.2691\ \mu\text{m} = 0.426\lambda_0$).

The simulations were performed at different resolutions. In order to make significant comparisons with respect to the isotropic case, the resolution is defined as

$$R = \frac{\lambda_{g1}}{\Delta} = \frac{1}{n^g_1}\frac{\lambda_0}{\Delta} \simeq 0.4R_0$$

where λ_{g1} is the wavelength of plane waves propagating along the principal axis of the guide and R_0 is the free-space resolution. The width of the guide was divided into 52 and 101 cells to obtain approximate resolutions of 10 and 20 cells per wavelength, respectively. The theoretical envelope of the fields is plotted in Fig. 8 compared to the numerical results obtained with the fourth-order method at $R \simeq 20$.

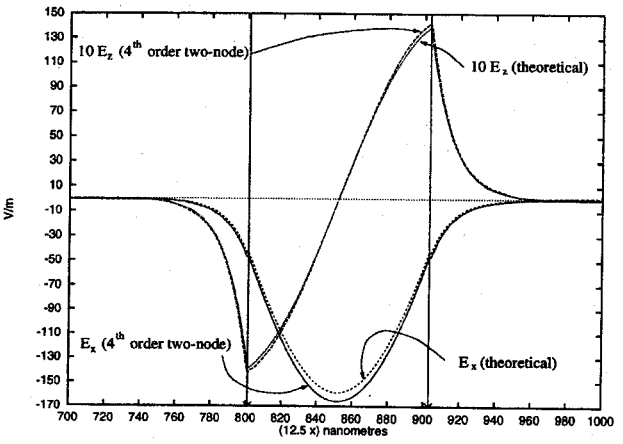

(a)

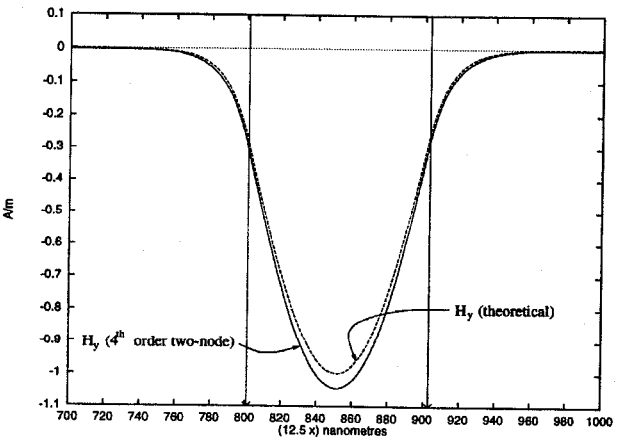

(b)

Fig. 8. Optical axis not in the plane of the slab. Theoretical and numerical results obtained with the fourth-order two-node scheme and a resolution in the guide of $R \simeq 20$.

Fig. 9 shows the envelope of the predominant component of the electric field (E_x) at $R \simeq 10$. The phase error has also

TABLE II
NUMERICAL VALUES OF THE NUMERICAL β FOR THE SECOND- AND FOURTH-ORDER TWO-NODE SCHEMES AT TWO DIFFERENT RESOLUTIONS, WHEN THE OPTICAL AXIS IS NOT IN THE PLANE OF THE SLAB

	Two-node (2^{nd})	Two-node (4^{th})
$R \simeq 20$	2.3429 10^7 (0.3%)	2.3334 10^7 (-0.07%)
$R \simeq 10$	2.3629 10^7 (1.2%)	2.3321 10^7 (-0.1%)

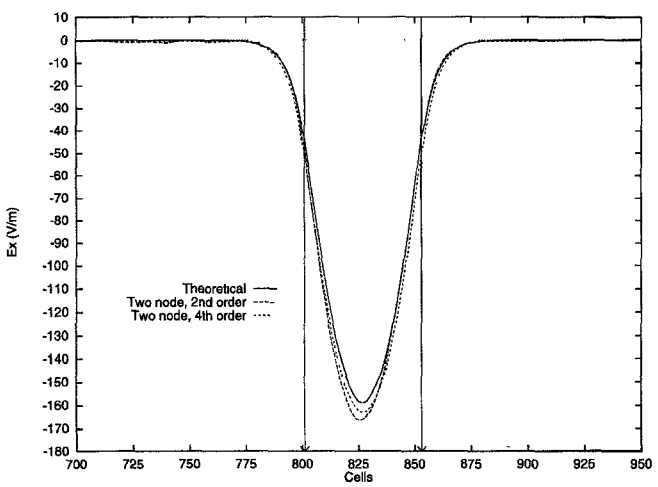

Fig. 9. Optical axis not in the plane of the slab. Comparison between the results obtained with the fourth-order two-node scheme, the second-order two-node scheme and the theoretical results. $R \simeq 10$. Envelope of E_x after 18.56 λ of propagation along the waveguide (200 cells).

been calculated and the numerical propagation constant then extracted from it (shown in Table II, with its relative error compared to the theoretical one).

The inclination angle of the H_y wavefront can be obtained, as is seen in (22), from $\arctan \sigma/\beta$ which in the theoretical case is $-1.86°$. The value of the numerical angle needs the numerical value of σ, which is obtained from the phase difference δ_φ in H_y by $\sigma_n = \delta_\varphi/\delta_x$, where δ_x is the horizontal separation between two points in the guide at a fixed z. The numerical inclination angle is $-1.92°$, *viz.*, it has an error of 4% with respect to the theory.

We have also evaluated the numerical errors both for the phase and the amplitude. The results obtained by the different schemes for the mean quadratic deviations between the theoretical and numerical amplitudes are not significant. Nevertheless, the phase error, especially in large problems solved with second order schemes, can become great enough to produce unacceptable results. Note that the choice of fourth-order methods allows the use of lower resolutions with smaller errors than higher resolutions for second-order methods. Furthermore the phase error of fourth-order algorithms increases more slowly than that of second-order ones when the resolution decreases.

B. Optical Axis in the Plane of the Slab

In this case, the fulfillment of the boundary conditions requires the mixture of ordinary and extraordinary waves. As can be seen in [28], the symmetric H_y modes are

$$E_x = \begin{cases} (B_{xo}e^{\gamma_o x} + B_{xe}e^{\gamma_e x})e^{-j\beta z}e^{j\omega t} \\ \quad \text{for } x < -d \\ (A_{xo}\cos(\kappa_o x) + A_{xe}\cos(\kappa_e x))e^{-j\beta z}e^{j\omega t} \\ \quad \text{for } |x| < d \\ (B_{xo}e^{-\gamma_o x} + B_{xe}e^{-\gamma_e x})e^{-j\beta z}e^{j\omega t} \\ \quad \text{for } x > d \end{cases}$$

$$E_y = \begin{cases} (B_{yo}e^{\gamma_o x} + B_{ye}e^{\gamma_e x})e^{-j\beta z}e^{j\omega t} \\ \quad \text{for } x < -d \\ A_{yo}\sin(\kappa_o x) + A_{ye}\sin(\kappa_e x))e^{-j\beta z}e^{j\omega t} \\ \quad \text{for } |x| < d \\ -(B_{yo}e^{-\gamma_o x} + B_{ye}e^{-\gamma_e x})e^{-j\beta z}e^{j\omega t} \\ \quad \text{for } x > d \end{cases}$$

$$E_z = \begin{cases} (B_{zo}e^{\gamma_o x} + B_{ze}e^{\gamma_e x})e^{-j\beta z}e^{j\omega t} \\ \quad \text{for } x < -d \\ (A_{zo}\sin(\kappa_o x) + A_{ze}\sin(\kappa_e x))e^{-j\beta z}e^{j\omega t} \\ \quad \text{for } |x| < d \\ -(B_{zo}e^{-\gamma_o x} + B_{ze}e^{-\gamma_e x})e^{-j\beta z}e^{j\omega t} \\ \quad \text{for } x > d. \end{cases}$$

The magnetic field is obtained from the electric field by

$$\vec{H} = \frac{j}{\omega\mu_0}\nabla \times \vec{E}.$$

The dispersion relations for the ordinary waves in the guide and cladding are

$$\kappa_o^2 = \omega^2\mu_0\varepsilon_1^g - \beta^2, \quad \gamma_o^2 = \beta^2 - \omega^2\mu_0\varepsilon_1^c$$

and those of the extraordinary wave are

$$\kappa_e^2 = \omega^2\mu_0\varepsilon_3^g - \beta^2\left(\sin^2\alpha + \frac{\varepsilon_3^g}{\varepsilon_1^g}\cos^2\alpha\right),$$

$$\gamma_e^2 = \beta^2\left(\sin^2\alpha + \frac{\varepsilon_3^c}{\varepsilon_1^c}\cos^2\alpha\right) - \omega^2\mu_0\varepsilon_3^c.$$

The four field amplitudes are obtained through the enforcement of the continuity of the tangential components in the guide-cladding boundaries. The equations thus obtained must be linearly independent so that the determinant of the coefficients is null. This results in a dispersion relation for the modes from which the roots β can be extracted.

The parameters of the guide are: $2d = 0.5$ μm, $\alpha = 20°$, $n_{co} = \sqrt{\varepsilon_1^c/\varepsilon_0} = 2.28$, $n_{ce} = \sqrt{\varepsilon_3^c/\varepsilon_0} = 2.17, \delta = 0.04$, $n_{go} = \sqrt{\varepsilon_1^g/\varepsilon_0} = 1.02n_{co}$ and $n_{ge} = \sqrt{\varepsilon_3^g/\varepsilon_0} = 1.02n_{ce}$.

The mode chosen corresponds to $\beta = 2.286 \cdot 10^7$ (wavelength $\lambda = 0.275$ μm $= 0.435\lambda_0$). The amplitudes and the wavenumber were obtained using Mathematica.

The simulations were performed at approximately the same resolutions as for the previous case: $R \simeq 10$ (20 cells for the width of the guide) and $R \simeq 20$ (40 cells for the width of the guide). The theoretical envelope of the fields is plotted in Fig. 10 and compared to the numerical results obtained with the fourth-order condensed two-node scheme at $R \simeq 20$.

Fig. 11 shows the results for the field envelope of the main component of the magnetic field (H_y) obtained with $R \simeq 10$, and Table III indirectly illustrates the phase errors showing the numerical propagation constants.

A good agreement between theoretical and computed results is achieved, even for the less energetic components of the

TABLE III
NUMERICAL VALUES OF THE NUMERICAL β FOR THE SECOND- AND FOURTH-ORDER TWO-NODE AND CONDENSED TWO-NODE SCHEMES AT TWO DIFFERENT RESOLUTIONS, WHEN THE OPTICAL AXIS IS IN THE PLANE OF THE SLAB

	Two–node (2^{nd})	Two–node (4^{th})	Cond. two–node (2^{nd})	Cond. two–node (4^{th})
$R \simeq 20$	2.2935 10^7 (0.3%)	2.2854 10^7 (-0.03%)	2.2940 10^7 (0.4%)	2.2862 10^7 (0.01%)
$R \simeq 10$	2.3153 10^7 (1.3 %)	2.2839 10^7 (-0.09%)	2.3181 10^7 (1.4%)	2.2866 10^7 (0.03%)

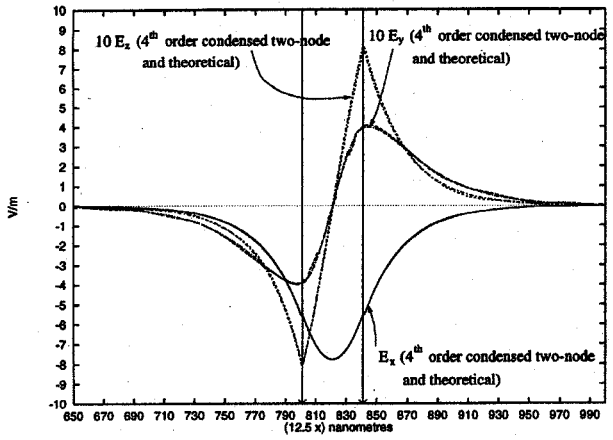

(a)

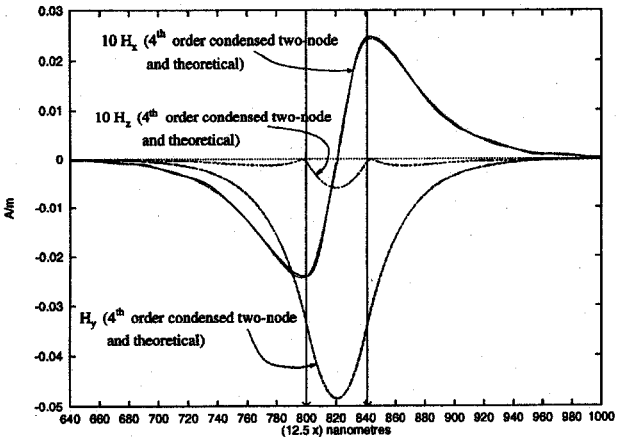

(b)

Fig. 10. Optical axis in the plane of the slab. Theoretical and numerical results obtained with the fourth-order condensed two-node scheme and a resolution in the guide of $R \simeq 20$.

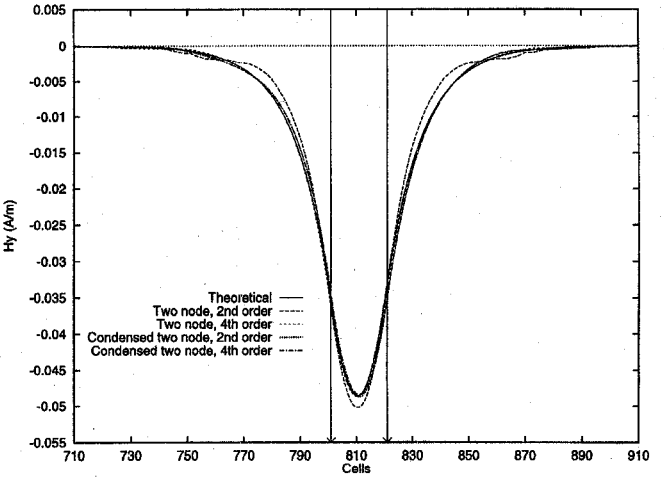

Fig. 11. Optical axis in the plane of the slab. Comparison between the results obtained with the fourth-order two-node scheme, the second-order two-node scheme, the fourth-order condensed two-node scheme, the second-order condensed two-node scheme, and the theoretical results. $R \simeq 10$. Envelope of H_x after 18.15 λ of propagation along the waveguide (200 cells).

fields. There are no significant differences from the amplitude point of view between the different methods at different resolutions, but the phase errors are significantly greater for the second order results, especially at low resolutions. Similar conclusions to those of the previous case may be drawn.

VII. CONCLUSION

This paper analyzes different ways of applying finite methods in the time domain to the simulation of electromagnetic wave propagation in inhomogeneous anisotropic media. An overview is given of some general principles for the construction of finite algorithms, similar to Yee's, but suitable for the treatment of anisotropic media. It is shown that a general set of finite operators approximating the partial derivatives to second and fourth order can be obtained that contain operators compatible with any regular distribution of components. Considering that the traditional FDTD scheme is based on a space-time distribution of the components and on the use of the basic centered differentiation operator, three approaches to the treatment of anisotropic media have been considered: choosing other operators, modifying the distribution, or both. Simple rules for the construction of the numerical schemes have been proposed that can easily be implemented through the use of symbolic languages such as Mathematica™.

Given that there are numerous possible schemes and that the performance of each is similar for the same order of approximation, the results presented here are limited to those of the schemes that use the same operator for all the spatial derivatives. Variants with second- and fourth-order approximation in space of the derivatives have been tested in every case. Testing was carried out by the simulation of single-mode propagation through planar anisotropic dielectric waveguides. The results obtained with moderate resolutions are satisfactory and fourth order schemes show smaller phase errors than second-order ones, which permits the use of lower resolutions or the treatment of larger problems for a given absolute error in the near-fields.

REFERENCES

[1] K. Yee, "Numerical solution of initial boundary problems in isotropic media," *IEEE Trans. Antennas Propagat.*, vol. 14, pp. 302–307, 1966.

[2] A. Taflove and K. R. Umashankar, "The finite-difference time-domain method for numerical modeling of electromagnetic wave interations with arbitrary structures," in *Progress in Electromagnetics Research. Finite Elements and Finite Difference Methods in Electromagnetic Scattering.* New York: Elsevier, 1990.
[3] P. A. Tirkas, C. A. Balanis, M. P. Pruchine, and G. C. Barber, "Finite-difference time-domain method for electromagnetic radiation, interference and interaction with complex structures," *IEEE Trans. Electromagn. Compat.*, vol. 35, no. 2, pp. 192–203, 1993.
[4] F. Hunsberger, R. J. Luebbers, and K. S. Kunz, "Finite-difference time-domain analysis of gyrotropic media—I: Magnetized plasma," *IEEE Trans. Antennas Propagat.*, vol. 40, pp. 1489–1495, 1992.
[5] S. T. Chu and S. K. Chaduri, "A finite-difference time-domain method for the design and analysis of guided-wave optical structures," *J. Lightwave Technol.*, vol. 7, no. 12, pp. 2033–2038, 1989.
[6] J. Fang, "Time domain finite difference computation for Maxwell's equations," Ph.D. dissertation, Univ. of California, Berkeley, 1989.
[7] M. T. Deveze, "Contribution á l'analyze, par différences finies, des équations de Maxwell dans le domaine temps." Ph.D. dissertation, Université de Paris, France, 1992.
[8] R. Mittra and P. Harms, "A new finite-difference time-domain (FDTD) algorithm for efficient field computation in resonator narrow band structures," *Microwave Guided Wave Lett.*, vol. 3, pp. 316–318, Sept. 1993.
[9] S. González García, "Contribuciones al método de las diferencias finitas para la resolución de las ecuaciones de Maxwell en el dominio del tiempo," Ph.D. dissertation, Univ. of Granada, Spain, Sept. 1994.
[10] J. Schneider and S. Hudson, "The finite-difference time-domain method applied to anisotropic material," *IEEE Trans. Antennas Propagat.*, vol. 41, no. 7, pp. 994–999, 1993.
[11] S. Xiao and R. Vahldieck, "An efficient 2-D FDTD algorithm using real variables," *IEEE Microwave Guided Wave Lett.*, vol. 3, no. 5, pp. 127–129, 1993.
[12] T. Materdey Bao-Hung, "Nueva formulación de métodos de diferencias finitas en el dominio del tiempo. Aplicación a guías dieléctricas anisótropas," Ph.D. dissertation, Univ. of Granada, Spain, Nov. 1993.
[13] T. Materdey, S. González, R. Gómez, and B. García, "A new vision of numerical methods for the solution of Maxwell's equations related to the FD-TD method. Application to general anisotropic media," in *Second Int. Conf. Computation in Electromagnetics*, Nottingham, U.K., Apr. 1994. IEE, pp. 138–141.
[14] Z. Bi, K. Wu, C. Wu, and J. Litva, "A new finite-difference time-domain algorithm for solving maxwell equations," *IEEE Microwave Guided Wave Lett.*, vol. 1, no. 12, pp. 382–384, 1991.
[15] M. Okoniewski, "Vector wave equation 2D-FDTD method for guided wave problems," *Microwave Guided Wave Lett.*, vol. 3, pp. 307–309, Sept. 1993.
[16] Z. Chen, M. M. Ney, and W. J. R. Hoefer, "A new finite-difference time-domain formulation and its equivalence with the TLM symmectrical condensed node," *IEEE Trans. Microwave Theory Tech.*, vol. 39, no. 12, pp. 2160–2169, 1991.
[17] A. Asi and L. Shafai, "Dispersion analysis of anisotropic inhomogeneus waveguides using compact 2D-FDTD," *Electron. Lett.*, vol. 28, no. 15, pp. 1451–1452, 1992.
[18] A. Reineix, T. Monediere, and F. Jecko, "Ferrite analysis using the finite-difference time-domain (FDTD) method," *Microwave Opt. Technol. Lett.*, vol. 5, no. 13, pp. 685–686, 1992.
[19] S. Xiao, R. Vahldieck, and H. Jin, "Full wave analysis of guided wave structures using a novel 2-D FDTD," *IEEE Microwave Guided Wave Lett.*, vol. 2, no. 5, pp. 165–167, 1992.
[20] T. Materdey, S. González, R. Gómez, and B. García, "Nuevos algoritmos de diferencias y promedios finitos en el dominio del tiempo para la solución de las ecuaciones de maxwell. Parte I: Medios isótropos," in *VIII Symp. Nacional URSI*, Valencia, Spain, 1993, pp. 635–639.
[21] ——, "Nuevos algoritmos de diferencias y promedios finitos en el dominio del tiempo para la solución de las ecuaciones de maxwell. Parte I: Medios anisótropos," in *VIII Symp. Nacional URSI*, Valencia, Spain, 1993, pp. 640–644.
[22] J. A. Pereda, L. A. Vielva, A. Vegas, and A. Prieto, "A treatment of magnetized ferrites using the FDTD method," *IEEE Microwave Guided Wave Lett.*, vol. 3, no. 5, pp. 136–138, 1993.
[23] J. A. Pereda, L. A. Vielva, A. Vegas, and A. Prieto, "FDTD analysis of magnetized ferrites: An approach based on the rotated Ritchmyer difference scheme," *IEEE Microwave Guided Wave Lett.*, vol. 3, no. 9, pp. 322–324, 1993.
[24] M. Okoniewski and E. Okoniewska, "FDTD anaylisis of magnetized ferrites: A more efficient algorithm," *IEEE Microwave Guided Wave Lett.*, vol. 4, pp. 169–171, June 1994.
[25] J. A. Pereda, "Extensión del método de diferencias finitas en el dominio del tiempo para el estudio de la propagación electromagnética en guías de onda cargadas con dieléctricos y ferritas magnetizadas," Ph.D. dissertation, Univ. of Cantabria, Santander, Spain, Mar. 1995.
[26] J. A. Pereda, L. A. Vielva, M. Solano, A. Vegas, and A. Prieto, "FDTD analysis of magnetized ferrites: Application to the calculation of dispersion characteristics of ferrite-loaded waveguides," *IEEE Trans. Microwave Theory Tech.*, vol. 43, pp. 350–357, Feb. 1995.
[27] D. Marcuse, "Modes of a symmetric slab optical waveguide in birefringent media—Part I: Optical axis not in plane of slab," *IEEE J. Quantum Electron.*, pp. 736–741, Oct. 1978.
[28] D. Marcuse and I. P. Kaminow, "Modes of a symmetric slab optical waveguide in birefringent media—Part II: Slab wih coplanar optical axis," *IEEE J. Quantum Electron.*, pp. 92–101, Feb. 1979.
[29] S. González García, T. M. Bao-Hung, B. García Olmedo, and R. Gómez Martín, "Volume conformation method to study scattering by PEC objects with FDTD," *IEE Proc. Microwaves, Antennas and Propagation*, Apr. 1996, pp. 131–136.
[30] S. González García, I. Villó Pérez, B. García Olmedo, and R. Gómez Martín, "On the applicability of the PML absorbing boundary condition to dielectric anisotropic media," *Electron. Lett.*, vol. 32, no. 14, pp. 1270–1271, 1996.

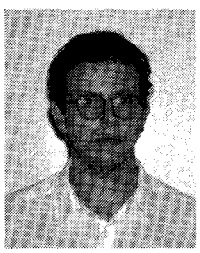

Salvador González García was born in Baeza, Spain, on May 13, 1966. He received the M.S. and Ph.D. (cum laude) degrees in physics from the University of Granada, Granada, Spain, in 1989 and 1994, respectively.

In 1989, he received a grant from the Spanish government, then became an Assistant Professor, University of Granada, in 1990. In 1996, he received a grant to work at the Institute of Mobil and Satellite Communication Techniques, Germany, for four months. His research interests include numerical electromagnetics, guided wave propagation, antenna theory, and time domain techniques.

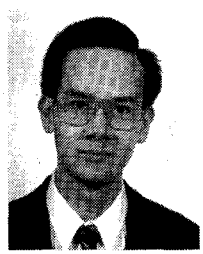

T. Materdey Hung-Bao received the B.S. and Ph.D. degrees in physics from the University of Granada, Granada, Spain, in 1990 and 1994, respectively.

He is the coauthor of a 3-D electromagnetic code for the Spanish aeronautic firm CASA based on the FDTD method. His research in Granada was sponsored by a fellowship from the Spanish government, and he is currently working on a research project at Cornell University, Ithaca, NY. His research interests include electromagnetic theory, numerical methods, and theoretical physics.

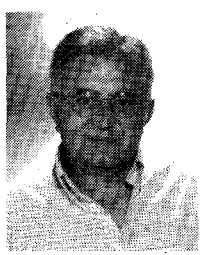

Rafael Gómez Martín received the M.S. degree from the University of Sevilla, Sevilla, Spain, in 1971 and the Ph.D. degree (cum laude) from the University of Granada, Granada, Spain, in 1974, all in physics.

From 1971 to 1974, he was with the University of Santiago de Compostela, Spain, as a Ph.D. student. From 1975 to 1985, he was an Associate Professor, University of Granada, where he became Professor in 1986. He is currently with the Department of Applied Physics, where he is responsible for Electromagnetics Group of Granada. His current research interest include the development of analytical and numerical methods in electromagnetism.

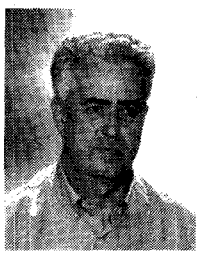

Bernardo García Olmedo was born in Granada, Spain, in 1940, and graduated in physics from the Universidad Complutense de Madrid, Madrid, Spain, in 1964. He undertook graduate studies at the University of California, Berkeley and received the Ph.D. degree from the Universidad de Sevilla, Sevilla, Spain, in 1968.

He has held different teaching posts at the University of Madrid, University of California, Berkeley, and Universidad de Sevilla. He has also been an Associate Professor, Universidad de Santiago de Compostela, and Professor, Universidad de Granada. His published works are related to hybrid electronic systems, special-purpose computers, signal processing, and, currently, numerical electromagnetics.

Dr. García is a member of the Real Sociedad Española de Física and the Real Academia de Ciencias of Granada.